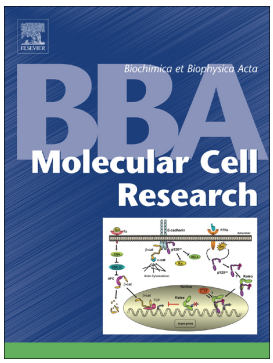

Upregulation of PD-L1 expression in breast cancer cells through the formation of 3D multicellular cancer aggregates under different chemical and mechanical conditions

Shohreh Azadi, Hamidreza Abolkheyr, Sajad Razavi Bazaz, Jean Paul Thiery, Mohsen Asadnia, Majid Ebrahimi Warkiani

PII: S0167-4889(19)30140-5

DOI: https://doi.org/10.1016/j.bbamcr.2019.118526

Reference: BBAMCR 118526

To appear in: *BBA - Molecular Cell Research*

Received date: 4 April 2019

Revised date: 20 July 2019

Accepted date: 4 August 2019

Please cite this article as: S. Azadi, H. Abolkheyr, S.R. Bazaz, et al., Upregulation of PD-L1 expression in breast cancer cells through the formation of 3D multicellular cancer aggregates under different chemical and mechanical conditions, *BBA - Molecular Cell Research*(2019), https://doi.org/10.1016/j.bbamcr.2019.118526

Upregulation of PD-L1 expression in breast cancer cells through the formation of 3D multicellular cancer aggregates under different chemical and mechanical conditions

Shohreh Azadi[1,2], Hamidreza Abolkheyr[1], Sajad Razavi Bazaz[1], Jean Paul Thiery[3], Mohsen Asadnia[2]

Majid Ebrahimi Warkiani[1,4*]

[1]School of Biomedical Engineering, University of Technology Sydney, Sydney, New South Wales 2007, Australia

[2]School of Engineering, Macquarie University, Sydney, 2109, Australia

[3]Inserm Unit 1186, Comprehensive Cancer Center, Institut Gustave Roussy, Villejuif, France

[4]Institute of Molecular Medicine, Sechenov University, Moscow, 119991, Russia

***** Contact

Majid Ebrahimi Warkiani (majid.Warkiani@uts.edu.au)

School of Biomedical Engineering, University Technology Sydney, Sydney, New South Wales 2007, Australia

Abstract

Expression of programmed death-ligand 1 (PD-L1) in cancer cells plays an important role in cancer-immune cell interaction. The emerging evidence suggests regulation of PD-L1 expression by several tumor microenvironmental cues. However, the association of PD-L1 expression with chemical and mechanical features of the tumor microenvironment, specifically epidermal growth factor receptor (EGFR) signaling and matrix stiffness, remains elusive. Herein, we determine whether EGFR targeting and substrate stiffness affect the regulation of PD-L1 expression. Breast carcinoma cell lines, MCF7 and MDA-MB-231, were cultured under different conditions targeting EGFR and exposing cells to distinct substrate stiffness to evaluate PD-L1 expression. Furthermore, the ability to form aggregates in short-term culture of breast carcinoma cells and its effect on expression level of PD-L1 was probed. Our results indicated that PD-L1 expression was altered in response to both EGFR inhibition and substrate stiffness. Additionally, a positive association between the formation of multicellular aggregates and PD-L1 expression was observed. MDA-MB-231 cells expressed the highest PD-L1 level on a stiff substrate, while inhibition of EGFR reduced expression of PD-L1. The results suggested that both physical and chemical features of tumor microenvironment regulate PD-L1 expression through alteration of tumor aggregate formation potential. In line with these results, the in-silico study highlighted a positive correlation between PD-L1 expression, EGFR signaling, epithelial to mesenchymal transition related transcription factors (EMT-TFs) and stemness markers in metastatic breast cancer. These findings improve our understanding of regulation of PD-L1 expression by tumor microenvironment leading to evasion of tumor cells from the immune system.

***Keywords*:** EGFR; Substrate stiffness; Immunotherapy; Cetuximab; PD-L1

1. Introduction

It is broadly understood that the tumor microenvironment (TME) and its interplay with cancer cells play a crucial role in tumor initiation, progression, metastasis, and drug response [1, 2]. A large number of studies highlighted the importance of non-cellular features of TME including extracellular matrix (ECM) and its stiffness in the induction of metastasis and drug resistance in various solid tumors [3-6]. The physical and chemical characteristics of TME can control the behavior and function of cancer cells [1, 7, 8]. Mechanical characteristics of TME changes during cancer progression expose tumor cells to different mechanical signals [9]. Variation of TME stiffness induced by cellular and non-cellular components is recognized as a pro-tumorigenic factor [10-12]. Activation of various oncogenic signaling pathways through the cellular and physical properties of TME has been reported previously, resulting in enhancing hypoxia, invasiveness, stemness and immune-escaping capability of cancer cells [13, 14].

During the past decade, immunotherapy has witnessed a revolution in cancer therapy with the development of immune checkpoint inhibitors, monoclonal antibodies against cytotoxic T lymphocyte antigen 4 (CTLA-4) and programmed cell death protein-1 (PD-1) or their ligands, including PD-1 ligand 1 (PD-L1) [15]. Emerging evidence highlighted roles of TME and ECM remodeling in regulating the cancer-immunity cycle [15-17]. However, the contribution of the ECM remodeling in shaping the immune microenvironment of the tumor is only beginning to be studied. Mechanical features of TME are increasingly recognized as crucial factors in immune cell trafficking, activation and immunological synapse formation [18]. The density of ECM and basement membrane composition are regulated by stromal matrix components and plays a crucial role in immune cell migration, spatial distribution, and activation of immune-escaping features of cancer cells [15, 17, 19]. Additionally, numerous growth factors secreted by tumor-supportive cells in TME can enhance the immune-

suppression capability of TME and immune-escaping potential of cancer cells. Recently several studies highlighted immune-modulatory effects and positive association of activation of epidermal growth factor receptor (EGFR) signaling with PD-L1 expression in TME [20, 21]. However, the association between matrix stiffness and EGFR on the expression of PD-L1 has not been elucidated.

There is a growing interest in the three-dimensional culture of cancer cells through the formation of 3D multicellular aggregates. Cellular aggregates display a variety of features which could better mimic the tumor microenvironment [22, 23]. An increasing number of studies demonstrated that the formation of tumor spheroids and cell aggregates could modulate numerous signaling pathways including stemness-related pathways [24-26]. Despite these studies, it is not yet been established whether the formation of cell aggregates can regulate the PD-L1 expression. This study was designed to determine whether the chemical and mechanical features of TME regulate the multicellular cancer aggregate (MCA) formation ability and PD-L1 expression in human breast cancer cells. Our findings postulated regulation of PD-L1 expression by EGFR signaling pathway, substrate stiffness, and MCA formation.

2. Materials and Methods

2.1 Cell culture

Cells of human breast cancer cell lines MCF7 (non-invasive) and MDA-MB-231 (highly invasive) were acquired from the University of Technology Sydney (UTS), Faculty of Science. The cells were maintained in the RPMI culture medium (ThermoFisher Scientific, USA) containing 10% fetal bovine serum (FBS) (ThermoFisher Scientific, USA) and supplemented with 1% L-glutamate (Thermo Fisher Scientific, USA) in an atmosphere of 5% CO2 and 95% air at 37 ºC. Both cell lines were cultured in five different study groups as

illustrated in figure 1, two as chemical groups and three as mechanical groups that referred to as non-treated, Cetuximab treated, stiff, semi-soft and soft substrates, respectively. Figure 1 presents a schematic illustration of workflow that will be described below.

2.2 Substrate preparation and characterization

To examine the effect of substrate stiffness on PD-L1 expression and the MCA formation ability of cancer cells, polydimethylsiloxane (PDMS) substrates with different stiffness were utilized. These substrates were prepared by mixing the silicone elastomer with the curing agent (Sylgard 184, Dow Corning, USA). Varying the ratio of elastomer to the curing agent allowed us to achieve PDMS substrates with different elastic modulus with negligible changes in other chemical and physical properties [27, 28]. Here we fabricated PDMS substrates by mixing silicone elastomer with the curing agent at a ratio of 10:1 and 50:1 and 75:1, to obtain stiff, semi-soft and soft substrates, respectively. Then, the mixture was degassed to expel bubbles and cured for 24 hours at 70°C. To ensure cell-substrate adhesion, synthesized substrates were treated via air plasma by a low-frequency plasma generator (230 V, Harrick Plasma, USA) at 30 W for 3 minutes, sterilized by UV for 30 minutes followed by coating with a thin layer of fibronectin (10μg/ml, Sigma-Aldrich, USA). Finally, the substrates were rinsed with PBS to remove excess protein and were immediately employed for cell seeding.

The substrate elasticity was measured by atomic force microscopy (AFM) indentation technique using a Nanowizard II atomic force microscope (JPK Instruments, Germany). The indentation was performed with V-shaped silicon nitride cantilever with a spring constant of 0.046 N/m (HYDRA6V-200NG, APPNANO, USA), at an approach velocity of 3 μm/s and a maximum indentation depth of 0.5 μm. For each substrate, three samples were prepared, and 70 to 100 force-displacement curves were recorded for each sample. The average Young's

moduli were calculated from at least 150-200 curves for each substrate (from three independent experiments) and reported as mean±SD. Briefly, in this technique, a flexible cantilever with a sharp tip indented the surface. During the indentation, the substrate-cantilever interaction led to a vertical deflection of the cantilever that was converted to the force and recorded against the indentation. The resulting force-indentation curve was used to obtain Young's modulus according to the modified Hertz model for a quadrilateral pyramid tip (equation 1) [29].

$$F(\delta) = \frac{1.49 E_{sub} tan\alpha}{2(1-\vartheta_{sub}^2)} \delta^2 \quad (1)$$

where, F is the force, δ is the indentation depth, and α is the half angle of pyramid tip which was set to 17.5°. The Poisson's ratio of substrates (ν_{sub}) was assumed to be 0.5 considering an incompressible material property for PDMS.

2.3 Anti-EGFR treatment

To assess the potential correlation between the PD-L1 protein expression with EGFR signaling and the MCA formation ability, the EGFR pathway was targeted by the anti-EGFR antibody Cetuximab (Merk, Germany). Cetuximab blocked EGFR through its binding to the extracellular domain of EGFR preventing receptor dimerization [30]. For immunostaining and ELISA, breast cancer cells were exposed to a culture medium supplemented with 10µg/ml Cetuximab for 48 hours. For MCA formation experiments, breast cancer cells were treated with the mentioned concentration of Cetuximab during the MCA formation process. The chosen concentration was below the reported peak plasma concentration of this drug [30, 31].

2.4 Evaluation of the PD-L1 expression

The PD-L1 expression of breast cancer cell lines was analyzed among different chemical and mechanical groups by immunofluorescence staining and enzyme-linked immunosorbent assay (ELISA). PD-L1 assessment was performed before and after formation of cellular aggregates.

2.4.1 Immunofluorescence staining of PD-L1

For PD-L1 immunostaining experiments, PDMS was spin-coated onto the glass slides at 2000 rpm for 30 seconds. Two types of breast cancer cells were cultured among five study groups. After 24 hours, the cells were fixed and permeabilized for 10 min with chilled 100% methanol (SigmaAldrich, USA). The fixation was followed by three times washing with phosphate-buffer saline (PBS) solution (ThermoFisher Scientific, USA) and blocking with 1% bovine serum albumin (BSA) (ThermoFisher Scientific, USA) in PBS for 60 min. Then, the cells were incubated with a rabbit monoclonal anti-PD-L1 antibody (dilution 1:100, ab209960, Abcam, USA) in PBS containing 1% BSA for overnight at 4ºC. Finally, the samples were washed and further incubated with 4,6-diamino-2-phenylindole (DAPI) (dilution 1:1000, D9542; SigmaAldrich, USA) for 5 min at room temperature. An inverted fluorescence microscope (Olympus IX71, USA) was utilized to capture the immunofluorescence images.

2.4.2 Measuring PD-L1 concentration using ELISA

The PD-L1 concentration was assessed among chemically and mechanically treated groups of the two breast carcinoma cell lines using quantitative ELISA kit (ab214565, Abcam, USA). ELISA was performed according to the manufacturer's instruction. First, cells were seeded at the concentration of 10^5 cells/ml on three PDMS substrates. The same number of cells were

cultured in non-treated and Cetuximab-treated groups. After 48 hours, the samples were extracted from the adherent cells and prepared according to the manufacturer's protocol. Briefly, the samples were added to the appropriate wells and incubated with the capture and detector antibodies for 1 hour at room temperature, then washed with the washing buffer followed by incubation with 3,3',5,5'-Tetramethylbenzidine (TMB) development solution and the stop solution. Finally, the optical density (OD) was recorded at 450 nm immediately after adding the stop solution. Eight standard samples with the pre-determined PD-L1 concentration were used to obtain a standard curve (data not shown). The standard curve was created by plotting the absorbance value for each standard concentration against the target protein concentration. This curve was fitted and employed to determine the concentration of PD-L1 protein in the samples. For each sample, three independent measurements were performed, and all the measurements were conducted in duplicate for statistical analysis.

2.5 MCA formation

2.5.1 Pre-treatment of the microwells before cell seeding

MCAs were formed using the microwell technique [23, 32, 33]. The 3D SpheroFilm™ microwell was obtained from Incyto Co. (Korea) with the inner diameter of 300 μm and the well depth of 300 μm. Each device consisted of 361 silicone elastomer microwells. To prepare the microwells for cell culturing, their surface was UV sterilized and pretreated with 100% ethanol (SigmaAldrich, USA) repeatedly pipetted to remove the air bubbles from the wells. Then the wells were washed three times with PBS by repeatedly pipetting and incubated with the cell culture medium overnight [34].

2.5.2 Cell seeding in the microwells

For each cell line, five SpheroFilm devices were used, two devices for non-treated and Cetuximab-treated cells and three devices for stiff, semi-soft and soft groups. First, breast cancer cells were cultured on the three mentioned PDMS substrates for 24 hours before introducing into the microwells. After removing the medium from the SpheroFilm devices, a total number of 1.4×10^6 breast cancer cells were distributed over the microwell surfaces of each group at the concentration of 2×10^5 cells/ml. After 15 minutes of cell seeding, the suspending cells were removed by aspiration, and fresh growth media was added. The medium was changed every day until the end of the MCA formation assay. For Cetuximab-treated group, the cells were exposed to the medium containing Cetuximab at the concentration of 10 μg/ml.

2.5.3 Isolation of the MCA from the microwells

After two days of culturing in the microwells, multicellular breast cancer aggregates were dislodged by pipetting growth medium onto the microwells, repeatedly. MCAs with the size of above 100 μm were obtained using a cell strainer with a pore size of 100 μm. After adding the MCAs, the strainer was flipped, and the growth medium was added to the bottom surface of strainer to collect the MCAs. The isolated MCAs were transferred to the appropriate wells or slides for further assessments.

2.6 MCA characterization

To evaluate the MCA formation ability of breast cancer cells with the different expression of PD-L1, the MCAs were characterized by performing live and dead assay, counting the number and diameter of formed MCAs, assessment of PD-L1 expression and MCA spreading.

2.6.1 Cell viability of MCA

MCAs were labeled directly in 48-well plates using a Cellstain double staining kit (Sigma Aldrich, USA) according to the manufacturer's protocol. The viable cells were labeled with Calcein-AM which stained the cytoplasm in green. Nuclei of the dead cells were labeled with propidium iodide in red. The MCAs were incubated in the assay solution (5 mL of PBS containing 10 μL of calcein-AM and 5 μL of propidium iodide) in each well for 15 minutes at 37˚C. The live/dead fluorescence images were captured using an inverted fluorescence microscope (Olympus IX71, USA).

2.6.2 Measurement of MCAs number and diameter

The formed MCAs among different groups were imaged using an Olympus IX71 inverted microscope. The total number of MCAs was determined by adding 400 μl of the final MCA suspension (4ml) in 48-well plate. The average diameter of MCAs was also calculated by measuring the diameter of at least 40 MCAs in each group. ImageJ (NIH, Bethesda, MD) was employed for number and diameter measurements [35]. Most of the MCAs presented a spherical shape. For those had ellipsoid shape, the longest dimension was measured as the diameter.

2.6.3 Immunofluorescence staining of PD-L1

To assess the PD-L1 expression in MCAs, isolated MCAs were stained with anti-PD-L1 antibody. First, the MCAs were fixed with chilled 100% methanol for 10 min at -20 ºC, then centrifuged at a speed of 1200 rpm for 5 min to remove methanol. The samples were washed with PBS followed by blocking with 1% BSA for 1 hour at room temperature. Then the MCAs were stained with a rabbit monoclonal PD-L1 antibody by overnight incubation at 4ºC. Later, the samples were washed three times with PBS to remove the unbound antibody.

Finally, the nuclei were stained with DAPI for 5 minutes and the images captured using an inverted fluorescent microscope.

2.7 MCAs spreading

Isolated MCAs were transferred to the 24-well plate and allowed to spread. The MCAs were monitored under a microscope to observe whether they attached to the surface. After the attachment of MCAs, the culture media was removed, and the fresh media added for the further cell aggregates cultivation and analysis. The PD-L1 expression of breast cancer cells in the spread MCAs was analyzed using the immunofluorescence staining of PD-L1 followed with measuring PD-L1 concentration by ELISA as described before.

To measure the PD-L1 concentration after formation of MCAs, first, MCAs were attached and spread for 24 hours, then spread MCAs were dissociated using trypsin (SigmaAldrich, USA) and the number of cells counted among five study groups of MCF7 and MDA-MB-231 spread aggregates. Finally, the counted cells were transferred to a new well at the concentration of 10^5 cells/ml and incubated for another 24 hours. ELISA was performed according to the manufacturer's instruction, as mentioned before.

2.8 The TCGA data analysis

The genomic alterations, co-expression, and correlation studies were performed on data from The Cancer Genome Atlas (TCGA), PanCancer Atlas Breast cancer database using TCGAWorkflow package under R-Software (version 3.8) and cBioportal (www.cbioportal.org). The protein-protein interaction analysis was performed by STRING PPI package under Cytoscape software (version 3.7.0).

2.9 Statistics

The results of quantitative experiments were expressed as mean±SD. The statistical analysis was performed with Student t-test. *p-value<0.05 was considered as a statistically significant and **p-value<0.005 was considered as an extremely significant. Microscopic images are representative images from three independent experiments. All Immunofluorescence staining experiments were repeated three times and three to five different sections were captured by fluorescent microscope for each sample. Data shown for the MCA diameter are the averages from at least 40 number of MCAs from three independent experiments. PD-L1 ELISA was conducted in three separate replicates as mentioned before.

3. Results

3.1 PDMS substrates elastic modulus

Three PDMS substrates with the different elastic moduli were achieved by controlling the ratio of polymer to the crosslinking agent. The elastic moduli of PDMS substrates with the ratio of 10:1, 50:1 and 75:1, were measured as 1.22±0.2 MPa, 32.38±2.2 kPa, and 5.10±0.4 kPa, respectively. These values cover the physiologically relevant elastic moduli of TME that are used to examine how the substrate rigidity affects the biological behavior of cancer cells [36, 37]. As mentioned, these substrates are referred to as stiff, semi-soft and soft in this paper.

3.2 Expression of PD-L1 protein in breast cancer cells

First, we determined the expression of PD-L1 protein in two breast cancer cell lines among five groups of non-treated, CTX-treated, stiff, semi-soft, and soft. Figure 2 exhibits the immunofluorescent images of PD-L1 and nucleus of breast cancer cells, which demonstrates that the degree of PD-L1 expression varies considerably among the study groups of breast

cancer cells. Consistent with the findings in the previous literature [38], high expression of PD-L1 protein was observed in MDA-MB-231 cells (figure 2B) whereas, there was a low expression of PD-L1 protein in MCF7 cells (figure 2A). To calculate the percentage of MDA-MB-231 cells with positive expression of PD-L1, the number of cells with positive PD-L1 fluorescent signal was counted and compared to the total number of cells in each figure using ImageJ (NIH, Bethesda, MD) [35]. The final values were calculated by averaging between three independent experiments for each study group. Application of anti-EGFR antibody for 24 hours significantly reduced the PD-L1 protein level in MDA-MB-231 cells from 92%±3% positive cells to 35%±6%, which revealed that the PD-L1 expression is positively related with the EGFR signaling. In addition, the effect of substrate stiffness on the PD-L1 expression was examined. The PD-L1 expression of MDA-MB-231 cells was affected not only by the chemical treatment but also by the substrate stiffness. Cancer cells on the stiff substrate expressed the most PD-L1 among three PDMS substrates with different rigidity. Substrate softening reduced the number of PD-L1 positive MDA-MB-231 cells from 74%±5% for the stiff substrate to 50%±6%, and 22%±3% for the semi-soft and soft substrates, respectively.

3.3 Characterization of the breast tumor MCAs

In this paper, MCA formation was performed in microwells. We screened the MCA formation ability of two breast cancer cells in five study groups. For all groups, the single cell suspension was seeded into the microwells, and most of the cellular aggregates reached above 100 µm after two days. The SpheroFilm device and MCA formation steps of two breast cancer cells are schematically illustrated in figure 3. Initially, cells settled in the bottom of microwells. After one day, the cells started to attach together and form cell aggregates. Later, on day 2, they formed denser 3D structures.

Initially, we examined the cell viability of MCAs and confirmed that both cell lines displayed more than 95% viability by Calcein AM staining (figure 4A) in all groups of study. Due to the small size of MCAs (less than 300 μm), the necrotic core was not observed in any of them. Next, we examined whether the EGFR targeting and substrate stiffening involved in the MCAs formation. The total number of formed MCAs and their average diameter are shown in figure 4 (B and C). We observed a considerable difference in the number and diameter across the formed aggregates. Although both breast cancer cells successfully formed MCAs, MDA-MB-231 cells were able to form more MCA with a larger size. The total number of formed aggregates in different groups of breast cancer cells has been displayed in figure 4, while table 1 reports the number of single cells versus aggregates to establish an MCA titer. This titer was calculated by dividing the number of formed aggregates by the number of single cells added to the SpheroFilm device. Our results revealed that Cetuximab treatment resulted in the alteration of MCA formation ability of breast cancer cells. The treated cells decreased MCA formation ability in terms of number and diameter which suggests that MCA formation of cancer cells strongly depends on the EGFR activity ($^{*}p<0.005$). MCA titer decreased from 1/5384 and 1/5000 for MCF7 and MDA-MB-231 cells in control groups to 1/7000 and 1/10000 in Cetuximab-treated groups, respectively.

Table 1. Aggregate formation ability of breast cancer cells in different chemical and mechanical groups. Values display MCA titer which is the number of formed MCAs per number of single cells

Group \ Cell	MCF7	MDA-MB-231
Non-treated	1/5384	1/5000
Treated	1/7000	1/10000
Stiff	1/6086	1/4000
Semi-soft	1/5833	1/6666
Soft	1/14000	1/7368

Furthermore, the MCA formation ability of both cancer cells was altered with the substrate stiffening. MCF7 and MDA-MB-231 cells cultured on the stiff substrates revealed more ability for MCA formation compared with the softer substrates ($^{*}p<0.05$). Although both cell lines respond to the substrate stiffness, non-invasive MCF7 cells showed more sensitivity than invasive MDA-MB-231 cells. The MCA titer of 1/6086 and 1/4000 in the stiff groups of MCF7 and MDA-MB-231 cells decreased to 1/14000 and 1/7368 in the soft groups, respectively. These changes were accompanied by a decrease in the average diameter of MCF7 MCAs from 200±43 μm to 167±54 μm by substrate softening ($^{*}p<0.05$).

Next, we examined whether PD-L1 is involved in the MCA formation induced by the EGFR blocking and substrate stiffening. Figure 5 provides representative immunofluorescent images of cancer aggregates, which reveals that MCA formation increased PD-L1 expression of breast cancer cells in the EGFR-dependent and stiffness-dependent manner. Breast MCAs from both cell lines characterized with the lower expression of PD-L1 in the soft group compared with the stiff group as well as the Cetuximab-treated group compared with the non-treated group. These results suggest an upregulation of PD-L1 through the formation of MCA, which is mediated by chemical and mechanical factors.

3.4 Assessment of the PD-L1 expression in spread breast MCA

Next, we further investigated whether MCA formation affects PD-L1 expression. Since MCAs are the 3D structures of hundreds of cells, their PD-L1 immunostaining would not be adequate to confirm the induction of PD-L1 expression by MCA formation. Therefore, we examined the PD-L1 expression of MCAs after spreading for 24 hours to permit the formation of a cell monolayer. Figure 6A, and B illustrate the spreading of cellular aggregates and formation of the monolayer, which consisted of those cancer cells that were successfully involved in the MCA formation. Additionally, to provide some quantitation, mean fluorescent

intensity (MFI) of MCF7 and MDA-MB-231 cells was analyzed using ImageJ from at least three independent imaging experiments for each group of study and has been reported in figure 6C. MCF7 cells showed an increased PD-L1 expression not only in the MCAs but also in the spread aggregates, which demonstrates induction of the PD-L1 expression by the MCA formation. Quantification of fluorescent intensity in figure 6C revealed a positive correlation between the substrate stiffness and the PD-L1 expression of MCF7 cells (*$p<0.05$). As shown before, the spread MCAs of MDA-MB-231 cells showed that the expression of PD-L1 is closely related to the EGFR activity. Moreover, the PD-L1 staining of MDA-MB-231 cells in figure 6 indicates the PD-L1 expression in the stiff substrate is more than the soft substrate but not the semi-soft substrate. This result is consistent with the concentration of PD-L1 from ELISA in figure 7B which confirms that PD-L1 concentrations in the stiff and semi-soft groups of MDA-MB-231 cells are very close to each other. Moreover, ELISA before MCA formation (figure 7A) demonstrated similar results for the stiff and semi-soft groups of MDA-MB-231 cells. These findings suggest that although MDA-MB-231 cells exhibited a substrate-dependent expression of PD-L1, they are more sensitive to the substrate stiffness in the range of 5 to 35 KPa which are related to semi-soft and soft substrates in this study.

To confirm the results of PD-L1 staining in figure 2, ELISA was employed to measure the PD-L1 concentration. In agreement with the PD-L1 staining results before multicellular formation, the PD-L1 concentration of MCF7 cells was measured below 30 pg/ml for all study groups (figure 7A). The PD-L1 protein concentration of invasive breast cancer cells (MDA-MB-231) was significantly reduced from 1898±62 pg/ml in the non-treated group to1341.6±110 pg/ml after EGFR targeting (*$p<0.05$). Similarly, the PD-L1 concentration of MDA-MB-231 cells grown on the soft substrate was significantly lower than those grown on the stiff substrate (*$p<0.05$). The values of 1620±29 pg/ml, 1500±49 pg/ml, and 1000±66 pg/ml were obtained for stiff, semi-soft, and soft substrates, respectively (figure 7A). The

above-mentioned results suggest that PD-L1 expression could be mediated by chemical and mechanical tumor microenvironmental cues.

To further confirm these results, the PD-L1 staining of spread aggregates was accompanied with measuring of PD-L1 concentration using ELISA (figure 7B). Among the five study groups of MCF7, we found the highest PD-L1 level in the non-treated group. In line with the data assessed by the immunofluorescent microscopy, MCF7 cells appeared as PD-L1 positive after MCA formation. Furthermore, the PD-L1 concentration of spread MCAs of MCF7 reached 214±28 pg/ml, 153±19 pg/ml and 151±24 pg/ml in stiff, semi-soft, and soft groups, respectively. In contrast, MDA-MB-231 cells did not exhibit a significant change in the PD-L1 concentration after MCA formation. In agreement with the previous results, spread aggregates of MDA-MB-231 cells exhibited noticeable PD-L1 expression mediated by EGFR blocking and substrate stiffening, so that Cetuximab treatment caused a decrease in PD-L1 expression in these cells.

3.5 The TCGA data analysis

The genomic alteration analysis shows that the basal subtype of breast cancer exhibits the highest expression and amplification of EGFR, PD-L1 (CD274) and PROM-1 compared to other subtypes (Figure 8A). Furthermore, positive correlation and co-expression between PD-L1 with EGFR, CD44 and epithelial to mesenchymal transition-related transcription factors (EMT-TFs) SNAI1, ZEB1 and TWIST1 were observed (Figure 8B). In line with these results, the protein-protein interaction analysis illustrated a direct interaction between PD-L1 and EGFR with stemness-related genes and EMT-TFs (Figure 8C).

4. Discussion

It is well established that the expression of PD-L1 plays an important role in cancer cell-mediated immune response. Expression of PD-L1 has been found in 5–40% tumor cells, helping tumor cells to escape from the immune elimination [39]. PD-L1 is one of the key molecular pathways used by tumor cells to engage T cell immune checkpoints. PD-L1 expressed on the surface of tumor cells binds to PD1, which is expressed by activated T cells, leading to bypassing immune checkpoints to evade immune recognition and protects tumor cells from T cell-mediated killing [40].

The cellular expression of PD-L1 could be affected by different chemical and mechanical factors of tumor microenvironment. Hence, identifying cellular and molecular mechanisms driving PD-L1 expression is crucial for the successful prediction of response to the PD-L1 targeted therapy. In this study, the effect of EGFR signaling and substrate stiffness, two important tumor microenvironmental factors on PD-L1 expression of breast cancer cells, was investigated. Further, we evaluated whether MCA formation of breast cancer cells could contribute to enhancing PD-L1 expression. It has been demonstrated that different cancer cell types express different levels of PD-L1 that could be associated with their invasive potential [41]. Kim *et al.* indicated that metastatic lung cancers express more PD-L1 as compared to the primary tumor [42]. A similar result was observed for breast cancer cells [38, 41]. Our finding also confirmed high PD-L1 expression of invasive MDA-MB-231 cells, while non-invasive MCF7 cells display a modest level of PD-L1 ($*p<0.05$).

Moreover, PD-L1 level of MDA-MB-231 cells is modulated by EGFR signaling and substrate stiffening. There are several studies which evaluated the effect of substrate stiffness on the cellular behavior of cancer cells [43, 44]. They cultured different types of cells usually on PDMS and Polyacrylamide gels with different elastic moduli in the range of KPa to MPa

[36, 37, 45]. In this study, choosing three different ratios of elastomer to curing agents for PDMS substrates resulted in the stiffness of 5KPa to 1MPa while the curing agent ratio was enough to achieve a complete polymerization process of PDMS. These range of stiffness is consistent with previously published data [46] and close to tumor stromal microenvironment [37, 47]. They reached the conclusion that cancer cells respond to the substrate rigidity by changing protein expression, proliferation, migration and differentiation ability. Most recently, Myazawa *et al.* probed the effect of substrate stiffness on the PD-L1 expression of lung cancer cells [48]. They demonstrated that substrate stiffening enhanced the PD-L1 level via actin-dependent mechanisms. Here, we investigated such a relationship by culturing breast cancer cells on stiff, semi-soft and soft PDMS substrates and demonstrated the relation between substrate stiffness and PD-L1 expression.

The association between EGFR and PD-L1 signaling pathways plays an important role in cancer targeted therapy and is gaining much more interest in recent years. Several studies evidenced a positive correlation between EGFR activity and PD-L1 expression [49, 50]. MDA-MB-231 cells have been shown to express a high level of EGFR, which render them as a suitable target for anti-EGFR treatment [51, 52]. EGFR is involved in the modulation of PD-L1 expression through AKT and STAT3 downstream signaling pathways [53, 54]. Regarding the correlation between these two important signaling pathways, much more attention has been paid for a combined targeting of EGFR and PD-L1 in recent years [55]. Our results indicated that EGFR-positive MDA-MB-231 cells expressed a high level of PD-L1, while EGFR-negative MCF7 cells did not show a significant level of PD-L1, which is in good agreement with previously published papers [38, 41]. Moreover, Cetuximab treatment of MDA-MB-231 cells was accompanied with a noticeable reduction of PD-L1, which further confirmed the relationship between PD-L1 expression and EGFR signaling pathway.

In line with these results, few preclinical studies on patients with advanced lung adenocarcinoma highlighted that acquired resistance to EGFR-TKIs can amplify the expression of PD-L1 and enhance immune escape in EGFR mutant lung adenocarcinoma in which targeting PD-L1 restored sensitivity of tumor cells to lymphocytes [56]. Interestingly, in a clinical study conducted by Lee and colleagues in EGFR-mutated lung adenocarcinomas patients treated with first-line EGFR-TKIs, the high tumor proportion score of PD-L1 negatively associated with the treatment response rate and the patient outcome, compared to EGFR-TKI sensitive tumor cells [57]. These results not only highlight a positive association between EGFR and PD-L1 expression, but also indicate the potential application of PDL-1 expression as a prognostic biomarker for patients with EGFR mutation.

There are various factors that could be influential in PD-L1 expression. It has been shown that PD-L1 contributes to cancer stemness, EMT and tumor invasion, albeit not focusing on EMT and stemness [50, 58, 59]. Noman *et al.* demonstrated that PD-L1 is upregulated through EMT activation of breast cancer cells by involving ZEB-1 and miR-200 [60]. Here, by analyzing data of invasive breast cancers from The Cancer Genome Atlas (TCGA) and protein-protein interaction, we illustrated a possible correlation between PD-L1 with EGFR, stemness-related genes, and EMT-TFs (Figure 8). In line with these results, Malta *et al.* reported a positive association between immune microenvironment content, PD-L1 levels and stemness features in breast cancer [59]. Additionally, the high expression of PD-L1 in $CD44^{+}$ breast cancer cells and its role in maintaining stemness factors including OCT-4A, Nanog and BMI1 have been reported [58, 61].

In this study, two approaches, substrate stiffness and EGFR targeting, were used to change the PD-L1 expression of breast cancer cells. It has been demonstrated that both approaches could activate EMT and alter stemness factors [62-64]. Abhold *et al.* reported a reduction of mesenchymal markers by EGFR targeting [63] while You *at el.* probed an enhancement of

stemness markers by substrate stiffening [62]. Regarding these studies, it can be concluded that both EGFR signaling and substrate stiffening could modulate the PD-L1 expression through the mediation of EMT and stemness.

Our results indicated the successful formation of breast MCAs in both cell lines among five study groups. However, noticeable differences were observed in the MCA formation ability of breast cancer cells in terms of MCA diameter and number. The effect of substrate stiffness on the various cellular behaviors has been investigated, while there is not any report addressing the effect of substrate stiffening on the MCA formation. For the first time, to our knowledge, we showed that cancer cells derived from the stiff substrate had a greater ability to form MCA. Furthermore, the MCA formation was influenced not only with the substrate stiffness but also with the EGFR activity. Cetuximab-treated MCF7 and MDA-MB-231 cells indicated a decrease of 23% and 50% respectively in the number of formed MCAs compared to non-treated cells, respectively. The average diameter of MCAs also decreased from the stiff to the soft substrate. Moreover, analyzing the number and diameter of breast cancer MCA revealed that their aggregate formation ability positively correlated with the PD-L1 expression level.

In this study, MCAs were formed to investigate how cancer aggregate formation could alter the PD-L1 expression of breast cancer cells. Overall, the assessment of PD-L1 level by immunostaining as well as ELISA indicated that firstly, MCAs derived from cells grown on the stiff substrate showed a higher level of PD-L1 among the three PDMS substrates, secondly, EGFR targeting decreased the PD-L1 level not only in the cancer cell monolayer but also in MCAs, and thirdly, the MCA formation considerably enhanced PD-L1 expression level of MCF7 cells.

Stemness markers could be affected by different mechanisms through spheroidogenesis of cancer cells [25]. Chen *et al.* reported that spheroid formation led to overexpression of stemness-related genes [65]. Moreover, it has been shown that formation of MCA could guide EMT shifting and collective cell invasion through Snail1, Vimentin, and E-cadherin gene expression alterations [66]. Furthermore, as discussed before, stemness markers and EMT process also correlate to PD-L1 expression. Our finding also demonstrated the association between MCA formation and PD-L1 expression. Taken together, our results suggest that the formation of MCAs could modulate the PD-L1 expression of MCF7 cells through the possible mediation of stemness markers and/or EMT factors.

Molecular targeted therapy (e.g., EGFR and Her2 inhibitors) and immunotherapy (e.g., PD1/PD-L1 inhibitors) are two of the most important approaches in cancer treatment. Unlike molecular targeted therapy, the prediction of response to immunotherapy faces more challenges. Although PD-L1 expression is widely used as a predictive biomarker to immunotherapy, to date, many immunotherapy treatments have demonstrated a low efficacy in most patients [67]. Our results indicate that even for PD-L1-negative cancer cells such as MCF7, PD-L1 expression could be altered by different cellular and molecular mechanisms, and in such a situation different therapeutic approaches should be considered. Therefore, successful prediction of response to immunotherapy, specifically PD-L1 targeting, requires much more experimentation in 2D and 3D microenvironments, under various chemical and mechanical conditions. Moreover, the correlation between EGFR and PD-L1 supports the approach of combination therapy as a more effective strategy to modulate cancer cell-immune cell interactions.

5. Conclusion

In summary, we showed that PD-L1 expression, an important biomarker of immunotherapy, is modulated by both substrate stiffness and EGFR activity. Further, we demonstrated that the PD-L1 expression level is associated with the formation of cellular aggregates. So, even for those cancer cells with a low level of PD-L1, the possible changes in the cancer cell- immune cell interaction should be considered. Overall, to achieve a successful prediction of response to immunotherapy, different influential chemical and mechanical factors should be examined. The evidence from this study has gone some way toward enhancing our understanding of factors which modulate the PD-L1 expression. Our findings suggest two possible relationships, firstly between the MCA formation and PD-L1 expression, and secondly, between PD-L1 expression and stemness/EMT markers which are involved in cancer progression. Further experiments will be required to determine which mechanisms underly the regulation of PD-L1 expression during the EMT and acquired stemness features.

Conflict of interest

No potential conflict of interest was reported by the authors.

References

[1] D.A. Senthebane, A. Rowe, N.E. Thomford, H. Shipanga, D. Munro, M.A. Al Mazeedi, H.A. Almazyadi, K. Kallmeyer, C. Dandara, M.S. Pepper, The role of tumor microenvironment in chemoresistance: To survive, keep your enemies closer, International journal of molecular sciences, 18 (2017) 1586.
[2] N.S. Nicholas, B. Apollonio, A.G. Ramsay, Tumor microenvironment (TME)-driven immune suppression in B cell malignancy, Biochimica et Biophysica Acta (BBA)-Molecular Cell Research, 1863 (2016) 471-482.
[3] J. Park, D.-H. Kim, H.-N. Kim, C.J. Wang, M.K. Kwak, E. Hur, K.-Y. Suh, S.S. An, A. Levchenko, Directed migration of cancer cells guided by the graded texture of the underlying matrix, Nature materials, 15 (2016) 792.
[4] M. Romero-López, A.L. Trinh, A. Sobrino, M.M. Hatch, M.T. Keating, C. Fimbres, D.E. Lewis, P.D. Gershon, E.L. Botvinick, M. Digman, Recapitulating the human tumor microenvironment: colon tumor-derived extracellular matrix promotes angiogenesis and tumor cell growth, Biomaterials, 116 (2017) 118-129.
[5] J.-W. Shin, D.J. Mooney, Extracellular matrix stiffness causes systematic variations in proliferation and chemosensitivity in myeloid leukemias, Proceedings of the National Academy of Sciences, 113 (2016) 12126-12131.
[6] J.J. Northey, L. Przybyla, V.M. Weaver, Tissue force programs cell fate and tumor aggression, Cancer discovery, 7 (2017) 1224-1237.
[7] L. Kass, J.T. Erler, M. Dembo, V.M. Weaver, Mammary epithelial cell: influence of extracellular matrix composition and organization during development and tumorigenesis, The international journal of biochemistry & cell biology, 39 (2007) 1987-1994.
[8] J.M. Muncie, V.M. Weaver, The Physical and Biochemical Properties of the Extracellular Matrix Regulate Cell Fate, Current topics in developmental biology, 130 (2018) 1-37.
[9] J.M. Northcott, I.S. Dean, J.K. Mouw, V.M. Weaver, Feeling Stress: The Mechanics of Cancer Progression and Aggression, Frontiers in cell and developmental biology, 6 (2018) 17.
[10] C.E. Barcus, E.C. Holt, P.J. Keely, K.W. Eliceiri, L.A. Schuler, Dense collagen-I matrices enhance pro-tumorigenic estrogen-prolactin crosstalk in MCF-7 and T47D breast cancer cells, PloS one, 10 (2015) e0116891.
[11] C.E. Barcus, K.A. O'Leary, J.L. Brockman, D.E. Rugowski, Y. Liu, N. Garcia, M. Yu, P.J. Keely, K.W. Eliceiri, L.A. Schuler, Elevated collagen-I augments tumor progressive signals, intravasation and metastasis of prolactin-induced estrogen receptor alpha positive mammary tumor cells, Breast Cancer Research, 19 (2017) 9.
[12] H.M. Brechbuhl, J. Finlay-Schultz, T.M. Yamamoto, A.E. Gillen, D.M. Cittelly, A.-C. Tan, S.B. Sams, M.M. Pillai, A.D. Elias, W.A. Robinson, Fibroblast subtypes regulate responsiveness of luminal breast cancer to estrogen, Clinical Cancer Research, 23 (2017) 1710-1721.
[13] C. Zhang, D. Samanta, H. Lu, J.W. Bullen, H. Zhang, I. Chen, X. He, G.L. Semenza, Hypoxia induces the breast cancer stem cell phenotype by HIF-dependent and ALKBH5-mediated m6A-demethylation of NANOG mRNA, Proceedings of the National Academy of Sciences, 113 (2016) E2047-E2056.
[14] R.J. Seager, C. Hajal, F. Spill, R.D. Kamm, M.H. Zaman, Dynamic interplay between tumour, stroma and immune system can drive or prevent tumour progression, Convergent science physical oncology, 3 (2017) 034002.
[15] M.U. Mushtaq, A. Papadas, A. Pagenkopf, E. Flietner, Z. Morrow, S.G. Chaudhary, F. Asimakopoulos, Tumor matrix remodeling and novel immunotherapies: the promise of matrix-derived immune biomarkers, Journal for immunotherapy of cancer, 6 (2018) 65.
[16] I.J. Cohen, R. Blasberg, Impact of the tumor microenvironment on tumor-infiltrating lymphocytes: focus on breast cancer, Breast cancer: basic and clinical research, 11 (2017) 1178223417731565.
[17] D.S. Chen, I. Mellman, Oncology meets immunology: the cancer-immunity cycle, Immunity, 39 (2013) 1-10.
[18] M. Huse, Mechanical forces in the immune system, Nature Reviews Immunology, 17 (2017) 679.

[19] R. Hallmann, X. Zhang, J. Di Russo, L. Li, J. Song, M.-J. Hannocks, L. Sorokin, The regulation of immune cell trafficking by the extracellular matrix, Current opinion in cell biology, 36 (2015) 54-61.
[20] R.A. Soo, S.M. Lim, N.L. Syn, R. Teng, R. Soong, T.S. Mok, B.C. Cho, Immune checkpoint inhibitors in epidermal growth factor receptor mutant non-small cell lung cancer: Current controversies and future directions, Lung Cancer, (2017).
[21] E.A. Akbay, S. Koyama, J. Carretero, A. Altabef, J.H. Tchaicha, C.L. Christensen, O.R. Mikse, A.D. Cherniack, E.M. Beauchamp, T.J. Pugh, Activation of the PD-1 pathway contributes to immune escape in EGFR-driven lung tumors, Cancer discovery, (2013) CD-13-0310.
[22] D. Lv, Z. Hu, L. Lu, H. Lu, X. Xu, Three‐dimensional cell culture: A powerful tool in tumor research and drug discovery, Oncology letters, 14 (2017) 6999-7010.
[23] T.Y. Tu, Z. Wang, J. Bai, W. Sun, W.K. Peng, R.Y.J. Huang, J.P. Thiery, R.D. Kamm, Rapid prototyping of concave microwells for the formation of 3D multicellular cancer aggregates for drug screening, Advanced healthcare materials, 3 (2014) 609-616.
[24] J.E. Ekert, K. Johnson, B. Strake, J. Pardinas, S. Jarantow, R. Perkinson, D.C. Colter, Three-dimensional lung tumor microenvironment modulates therapeutic compound responsiveness in vitro–implication for drug development, PloS one, 9 (2014) e92248.
[25] T. Ishiguro, H. Ohata, A. Sato, K. Yamawaki, T. Enomoto, K. Okamoto, Tumor-derived spheroids: relevance to cancer stem cells and clinical applications, Cancer science, 108 (2017) 283-289.
[26] D.S. Reynolds, K.M. Tevis, W.A. Blessing, Y.L. Colson, M.H. Zaman, M.W. Grinstaff, Breast Cancer Spheroids Reveal a Differential Cancer Stem Cell Response to Chemotherapeutic Treatment, Scientific reports, 7 (2017) 10382.
[27] M.S. Yousafzai, G. Coceano, S. Bonin, J. Niemela, G. Scoles, D. Cojoc, Investigating the effect of cell substrate on cancer cell stiffness by optical tweezers, Journal of biomechanics, 60 (2017) 266-269.
[28] M. Prager-Khoutorsky, A. Lichtenstein, R. Krishnan, K. Rajendran, A. Mayo, Z. Kam, B. Geiger, A.D. Bershadsky, Fibroblast polarization is a matrix-rigidity-dependent process controlled by focal adhesion mechanosensing, Nature cell biology, 13 (2011) 1457.
[29] F. Rico, P. Roca-Cusachs, N. Gavara, R. Farré, M. Rotger, D. Navajas, Probing mechanical properties of living cells by atomic force microscopy with blunted pyramidal cantilever tips, Physical Review E, 72 (2005) 021914.
[30] S. Azadi, M. Tafazzoli-Shadpour, R. Omidvar, L. Moradi, M. Habibi-Anbouhi, Epidermal growth factor receptor targeting alters gene expression and restores the adhesion function of cancerous cells as measured by single cell force spectroscopy, Molecular and cellular biochemistry, 423 (2016) 129-139.
[31] A. Cavazzoni, R.R. Alfieri, D. Cretella, F. Saccani, L. Ampollini, M. Galetti, F. Quaini, G. Graiani, D. Madeddu, P. Mozzoni, Combined use of anti-ErbB monoclonal antibodies and erlotinib enhances antibody-dependent cellular cytotoxicity of wild-type erlotinib-sensitive NSCLC cell lines, Molecular cancer, 11 (2012) 91.
[32] A. Kang, H.I. Seo, B.G. Chung, S.-H. Lee, Concave microwell array-mediated three-dimensional tumor model for screening anticancer drug-loaded nanoparticles, Nanomedicine: Nanotechnology, Biology and Medicine, 11 (2015) 1153-1161.
[33] Y. Jo, N. Choi, H.N. Kim, J. Choi, Probing characteristics of cancer cells cultured on engineered platforms simulating different microenvironments, Artificial cells, nanomedicine, and biotechnology, (2018) 1-10.
[34] Y. Wang, M.H. Kim, S.R. Tabaei, J.H. Park, K. Na, S. Chung, V.P. Zhdanov, N.-J. Cho, Spheroid formation of hepatocarcinoma cells in microwells: experiments and Monte Carlo simulations, PloS one, 11 (2016) e0161915.
[35] C.T. Rueden, J. Schindelin, M.C. Hiner, B.E. DeZonia, A.E. Walter, E.T. Arena, K.W. Eliceiri, ImageJ2: ImageJ for the next generation of scientific image data, BMC bioinformatics, 18 (2017) 529.
[36] C. Rianna, M. Radmacher, Influence of microenvironment topography and stiffness on the mechanics and motility of normal and cancer renal cells, Nanoscale, 9 (2017) 11222-11230.

[37] J.R. Staunton, W. Vieira, K.L. Fung, R. Lake, A. Devine, K. Tanner, Mechanical properties of the tumor stromal microenvironment probed in vitro and ex vivo by in situ-calibrated optical trap-based active microrheology, Cellular and molecular bioengineering, 9 (2016) 398-417.
[38] E.-M. Rom-Jurek, N. Kirchhammer, P. Ugocsai, O. Ortmann, A.K. Wege, G. Brockhoff, Regulation of Programmed Death Ligand 1 (PD-L1) Expression in Breast Cancer Cell Lines In Vitro and in Immunodeficient and Humanized Tumor Mice, International journal of molecular sciences, 19 (2018) 563.
[39] Y. Wang, H. Wang, H. Yao, C. Li, J.-Y. Fang, J. Xu, Regulation of PD-L1: emerging routes for targeting tumor immune evasion, Frontiers in pharmacology, 9 (2018).
[40] F.L. Ricklefs, Q. Alayo, H. Krenzlin, A.B. Mahmoud, M.C. Speranza, H. Nakashima, J.L. Hayes, K. Lee, L. Balaj, C. Passaro, Immune evasion mediated by PD-L1 on glioblastoma-derived extracellular vesicles, Science advances, 4 (2018) eaar2766.
[41] H. Soliman, F. Khalil, S. Antonia, PD-L1 expression is increased in a subset of basal type breast cancer cells, PloS one, 9 (2014) e88557.
[42] S. Kim, J. Koh, D. Kwon, B. Keam, H. Go, Y.A. Kim, Y.K. Jeon, D.H. Chung, Comparative analysis of PD-L1 expression between primary and metastatic pulmonary adenocarcinomas, European Journal of Cancer, 75 (2017) 141-149.
[43] J. Raczkowska, S. Prauzner-Bechcicki, Discrimination between HCV29 and T24 by controlled proliferation of cells co-cultured on substrates with different elasticity, Journal of the mechanical behavior of biomedical materials, 88 (2018) 217-222.
[44] S. Prauzner-Bechcicki, J. Raczkowska, E. Madej, J. Pabijan, J. Lukes, J. Sepitka, J. Rysz, K. Awsiuk, A. Bernasik, A. Budkowski, PDMS substrate stiffness affects the morphology and growth profiles of cancerous prostate and melanoma cells, Journal of the mechanical behavior of biomedical materials, 41 (2015) 13-22.
[45] V. Shukla, N. Higuita-Castro, P. Nana-Sinkam, S. Ghadiali, Substrate stiffness modulates lung cancer cell migration but not epithelial to mesenchymal transition, Journal of Biomedical Materials Research Part A, 104 (2016) 1182-1193.
[46] A. Ansardamavandi, M. Tafazzoli-Shadpour, M.A. Shokrgozar, Behavioral remodeling of normal and cancerous epithelial cell lines with differing invasion potential induced by substrate elastic modulus, Cell adhesion & migration, 12 (2018) 472-488.
[47] J.G. Goetz, S. Minguet, I. Navarro-Lérida, J.J. Lazcano, R. Samaniego, E. Calvo, M. Tello, T. Osteso-Ibáñez, T. Pellinen, A. Echarri, Biomechanical remodeling of the microenvironment by stromal caveolin-1 favors tumor invasion and metastasis, Cell, 146 (2011) 148-163.
[48] A. Miyazawa, S. Ito, S. Asano, I. Tanaka, M. Sato, M. Kondo, Y. Hasegawa, Regulation of PD-L1 expression by matrix stiffness in lung cancer cells, Biochemical and biophysical research communications, 495 (2018) 2344-2349.
[49] K. Takada, G. Toyokawa, T. Tagawa, K. Kohashi, M. Shimokawa, T. Akamine, S. Takamori, F. Hirai, F. Shoji, T. Okamoto, PD-L1 expression according to the EGFR status in primary lung adenocarcinoma, Lung Cancer, 116 (2018) 1-6.
[50] P. Dong, Y. Xiong, J. Yue, S.J. Hanley, H. Watari, Tumor-intrinsic PD-L1 signaling in cancer initiation, development and treatment: beyond immune evasion, Frontiers in oncology, 8 (2018).
[51] E. Kumaraswamy, K.L. Wendt, L.A. Augustine, S.R. Stecklein, E.C. Sibala, D. Li, S. Gunewardena, R.A. Jensen, BRCA1 regulation of epidermal growth factor receptor (EGFR) expression in human breast cancer cells involves microRNA-146a and is critical for its tumor suppressor function, Oncogene, 34 (2015) 4333.
[52] T. Tanei, D.S. Choi, A.A. Rodriguez, D.H. Liang, L. Dobrolecki, M. Ghosh, M.D. Landis, J.C. Chang, Antitumor activity of Cetuximab in combination with Ixabepilone on triple negative breast cancer stem cells, Breast Cancer Research, 18 (2016) 6.
[53] N. Zhang, Y. Zeng, W. Du, J. Zhu, D. Shen, Z. Liu, J.-A. Huang, The EGFR pathway is involved in the regulation of PD-L1 expression via the IL-6/JAK/STAT3 signaling pathway in EGFR-mutated non-small cell lung cancer, International journal of oncology, 49 (2016) 1360-1368.
[54] T. Sasada, K. Azuma, J. Ohtake, Y. Fujimoto, Immune responses to epidermal growth factor receptor (EGFR) and their application for cancer treatment, Frontiers in pharmacology, 7 (2016) 405.

[55] I. Moya-Horno, S. Viteri, N. Karachaliou, R. Rosell, Combination of immunotherapy with targeted therapies in advanced non-small cell lung cancer (NSCLC), Therapeutic advances in medical oncology, 10 (2018) 1758834017745012.
[56] S. Peng, Q. Li, W. Wang, Acquired resistance to EGFR-TKI upregulates the expression of PD-L1 and promotes immune escape in lung cancer, AACR, 2017.
[57] W. Jeon, B. Lim, S. Han, W. Kwack, B. Chang, H. Choi, Y. Kim, C. Choi, M. Park, J.-H. Yoo, Positive PD-L1 Expression Is Associated with Unfavorable Clinical Outcome in EGFR-Mutated Lung Adenocarcinomas Treated with EGFR-TKIs, D110. LUNG CANCER: OPTIMIZING SCREENING, DIAGNOSIS, AND TREATMENT, American Thoracic Society, Place Published, 2019, pp. A7291-A7291.
[58] A. Alsuliman, D. Colak, O. Al-Harazi, H. Fitwi, A. Tulbah, T. Al-Tweigeri, M. Al-Alwan, H. Ghebeh, Bidirectional crosstalk between PD-L1 expression and epithelial to mesenchymal transition: significance in claudin-low breast cancer cells, Molecular cancer, 14 (2015) 149.
[59] T.M. Malta, A. Sokolov, A.J. Gentles, T. Burzykowski, L. Poisson, J.N. Weinstein, B. Kamińska, J. Huelsken, L. Omberg, O. Gevaert, Machine learning identifies stemness features associated with oncogenic dedifferentiation, Cell, 173 (2018) 338-354. e315.
[60] M.Z. Noman, B. Janji, A. Abdou, M. Hasmim, S. Terry, T.Z. Tan, F. Mami-Chouaib, J.P. Thiery, S. Chouaib, The immune checkpoint ligand PD-L1 is upregulated in EMT-activated human breast cancer cells by a mechanism involving ZEB-1 and miR-200, Oncoimmunology, 6 (2017) e1263412.
[61] S. Almozyan, D. Colak, F. Mansour, A. Alaiya, O. Al-Harazi, A. Qattan, F. Al-Mohanna, M. Al-Alwan, H. Ghebeh, PD-L1 promotes OCT4 and Nanog expression in breast cancer stem cells by sustaining PI3K/AKT pathway activation, International journal of cancer, 141 (2017) 1402-1412.
[62] Y. You, Q. Zheng, Y. Dong, X. Xie, Y. Wang, S. Wu, L. Zhang, Y. Wang, T. Xue, Z. Wang, Matrix stiffness-mediated effects on stemness characteristics occurring in HCC cells, Oncotarget, 7 (2016) 32221.
[63] E.L. Abhold, A. Kiang, E. Rahimy, S.Z. Kuo, J. Wang-Rodriguez, J.P. Lopez, K.J. Blair, M.A. Yu, M. Haas, K.T. Brumund, EGFR kinase promotes acquisition of stem cell-like properties: a potential therapeutic target in head and neck squamous cell carcinoma stem cells, PloS one, 7 (2012) e32459.
[64] A. Rice, E. Cortes, D. Lachowski, B. Cheung, S. Karim, J. Morton, A. Del Rio Hernandez, Matrix stiffness induces epithelial–mesenchymal transition and promotes chemoresistance in pancreatic cancer cells, Oncogenesis, 6 (2017) e352.
[65] C. Chen, Y. Wei, M. Hummel, T.K. Hoffmann, M. Gross, A.M. Kaufmann, A.E. Albers, Evidence for epithelial-mesenchymal transition in cancer stem cells of head and neck squamous cell carcinoma, PloS one, 6 (2011) e16466.
[66] A.S. Piotrowski-Daspit, J. Tien, C.M. Nelson, Interstitial fluid pressure regulates collective invasion in engineered human breast tumors via Snail, vimentin, and E-cadherin, Integrative Biology, 8 (2016) 319-331.
[67] C.L. Ventola, Cancer immunotherapy, part 3: Challenges and future trends, Pharmacy and Therapeutics, 42 (2017) 514.

Figure Captions

Figure. 1 Schematic illustration of the workflow. Breast cancer cells were cultured among chemical and mechanical study groups and assessed for PD-L1 expression before and after formation of multicellular aggregates.

Figure. 2 Regulation of PD-L1 expression by EGFR signaling and substrate stiffening. Representative immunofluorescent images of **(A)** MCF7 and **(B)** MDA-MB-231 cells cultured on non-treated, EGFR treated, stiff, semi-soft, and soft groups for 24 hours, stained for PD-L1 (red) and nuclei (blue). Images were obtained using an inverted fluorescent microscope. Scale bar denotes 50 µm and experiments were repeated three times.

Figure. 3 Schematic of the SpheroFilm utilized to generate multicellular cancer aggregates (MCAs) and representative images of the MCA formation of breast cancer cells. Scale bar is 100 µm. (I) Side view of the SpheroFilm contains 361 microwells with a diameter of 300 µm, and depth of 300 µm **(II)** Breast cancer cells were seeded into the microwells (day 0) among five study groups of non-treated, CTX-treated, stiff, semi-soft, and soft **(III)** The cancer cells grouped together to form cell aggregates after 1 day **(IV)** Cell aggregates formed dense 3D spherical structures after 2 days **(V)** MCAs were isolated from SpheroFilm and strained with a 100µm pore filter.

Figure. 4 MCA characterization. (A) live and dead assay reveals excellent viability of 3D MCAs of MCF7 and MDA-MB-231 cells among five chemical and mechanical treated groups. The live cells were stained with Calcein AM (Green), and the dead cells were stained with PI (Red), as described in materials and methods. Arrows show some of dead cells. The images were obtained by fluorescent microscopy with a scale bar of 100 µm. **(B and C)** Number and diameter of MCAs with **(B)** MCF7 and **(C)** MDA-MB-231 cells. The number of MCAs has been represented as the mean ± SD of three independent experiments. The mean diameter of MCAs has been represented as the mean ± SD of at least 40 MCAs in each group.

Figure. 5 Role of the MCA formation in the PD-L1 expression of breast cancer cells. Representative bright field and immunofluorescence images of **(A)** MCF7 and **(B)** MDA-MB-231 MCAs in five study groups of non-treated, CTX-treated, stiff, semi-soft, and soft, stained for PD-L1 (red) and nuclei (blue). Images were obtained using a fluorescent microscope, and scale bar denotes 50 µm and experiments were repeated three times.

Figure. 6 PD-L1 expression of spread MCAs of breast cancer cells as a function of EGFR activity and substrate stiffness. Representative bright field and immunofluorescence images of **(A)** MCF7 and **(B)** MDA-MB-231 MCAs in five study groups which were stained for PD-L1 (red) and nuclei (blue). Images were obtained using a fluorescent microscope. Scale bar represents 100 µm and experiments were repeated three times. **(C)** Mean fluorescent intensity was analyzed using ImageJ. The values are mean ± SD of three independent experiments. *significantly different between the groups ($p < 0.05$) and ** ($p < 0.005$).

Figure. 7 Comparison of protein concentration of PD-L1 in the chemical and mechanical groups, before and after formation of MCAs. The PD-L1 concentration of two breast cancer cell lines, MCF7 and MDA-MB-231 cells was measured by ELISA among five study groups of non-treated, Cetuximab treated, stiff, semi-soft, and soft substrates **(A)** before

and **(B)** after MCA formation. The values are mean ± SD of three independent experiments with duplicate measurements for each. * significantly different between the groups ($p < 0.05$) and ** ($p < 0.005$).

Figure. 8 Genomic and protein-protein interaction analysis of PD-L1. **(A)** The TCGA Pan-Breast Cancer Atlas genomic analysis. The oncoprint data shows amplification and up-regulation of PD-L1, EGFR, and PROM-1 in Basal subtype of breast cancer compared to other subtypes. **(B)** Co-expression and correlation analysis of PD-L1 expression with EGFR, CD44, and core EMT-TFs **(C)** protein-protein network interaction between PD-L1, EGFR and panel of candidate stemness genes and EMT-TFs in breast cancer.

Highlights

- Matrix stiffness regulates PD-L1 expression in breast cancer cells
- PD-L1 expression level is strongly influenced by EGFR signaling
- Formation of multicellular aggregates induces PD-L1 expression in breast cancer cells
- There is a positive correlation between PD-L1 with EGFR, EMT factors and stemness markers

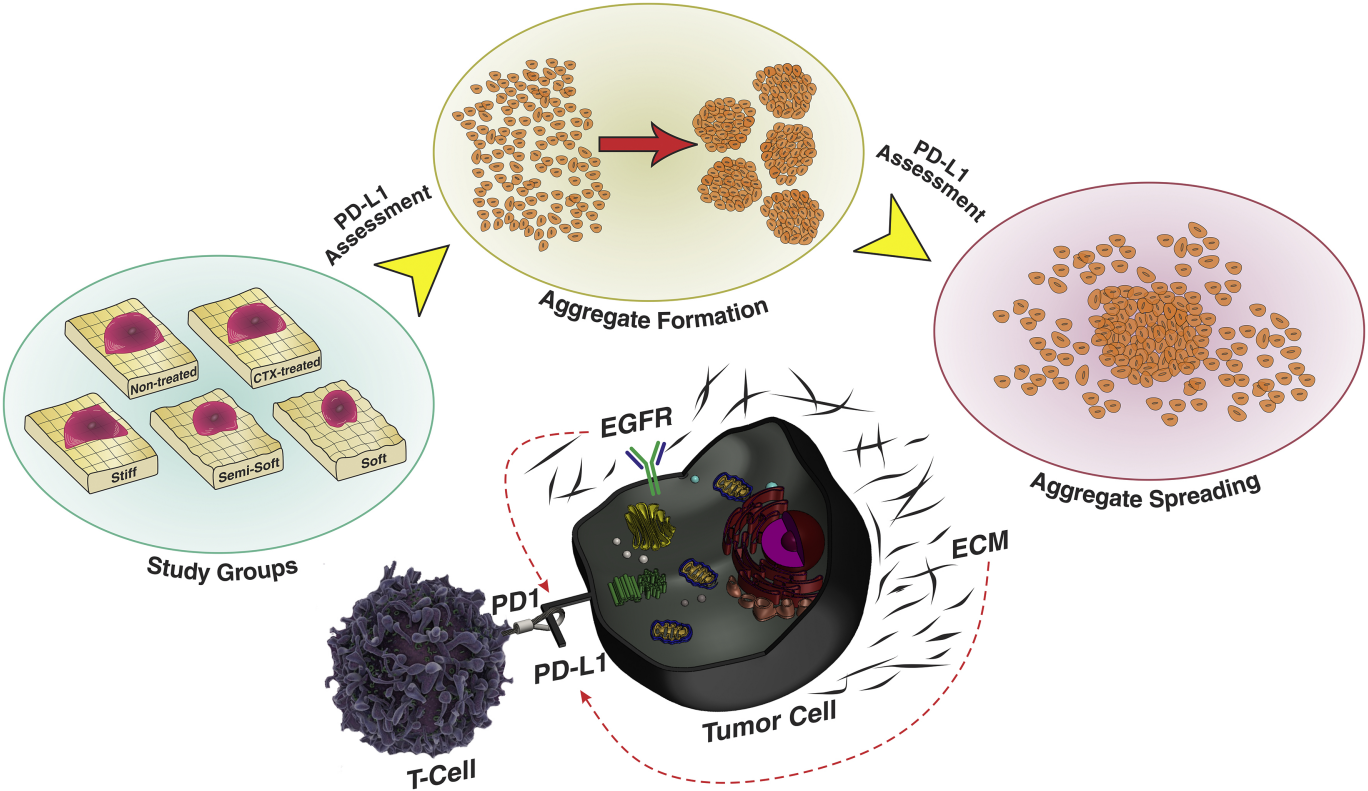
PD-L1
Assessment
Aggregate Formation
PD-L1
Assessment
Aggregate Spreading
Non-treated
CTX-treated
Stiff
Semi-Soft
Soft
Study Groups
EGFR
ECM
PD1
PD-L1
Tumor Cell
T-Cell

Figure 1

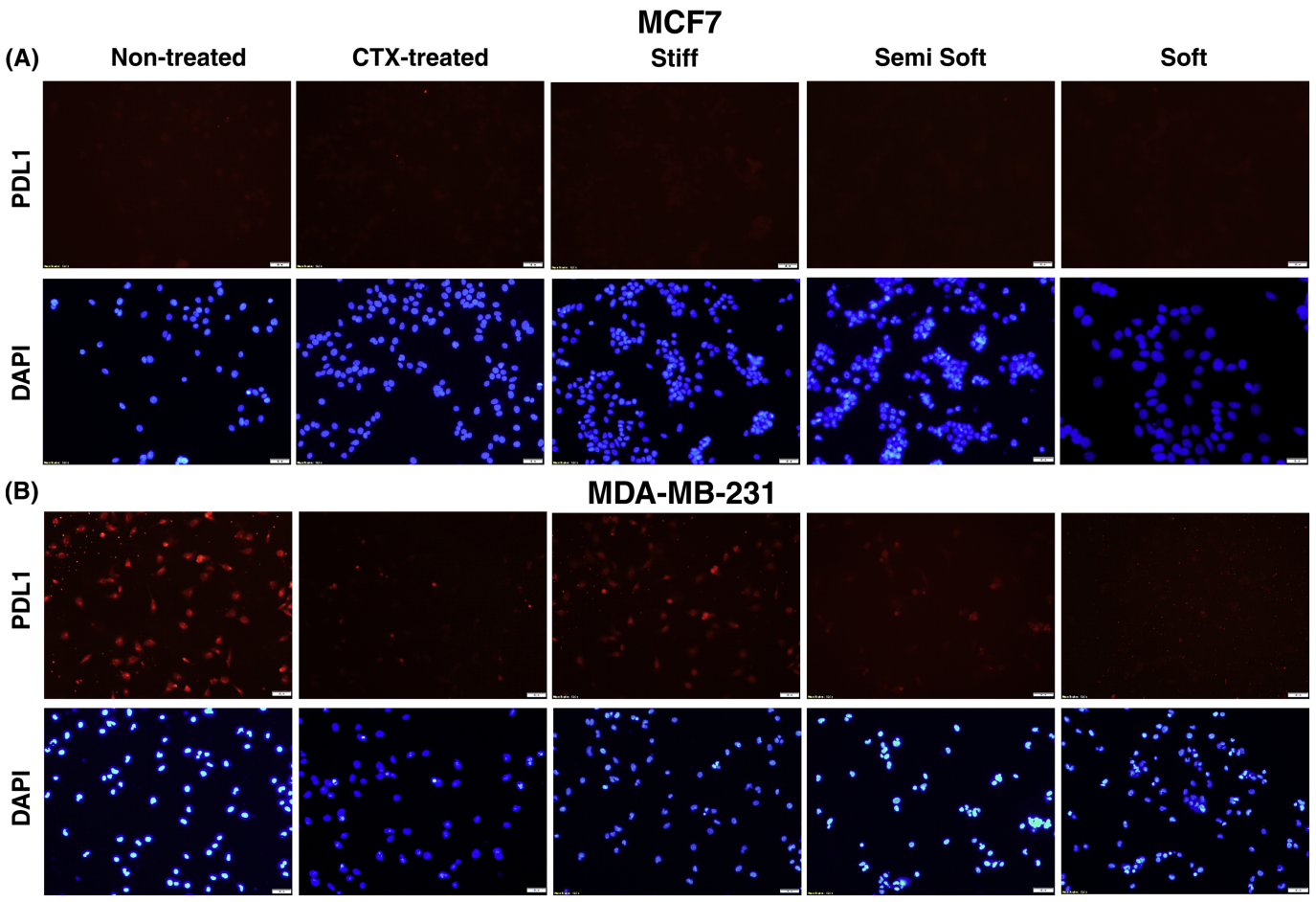
MCF7
(A)
Non-treated
CTX-treated
Stiff
Semi Soft
Soft
PDL1
DAPI
(B)
MDA-MB-231
PDL1
DAPI

Figure 2

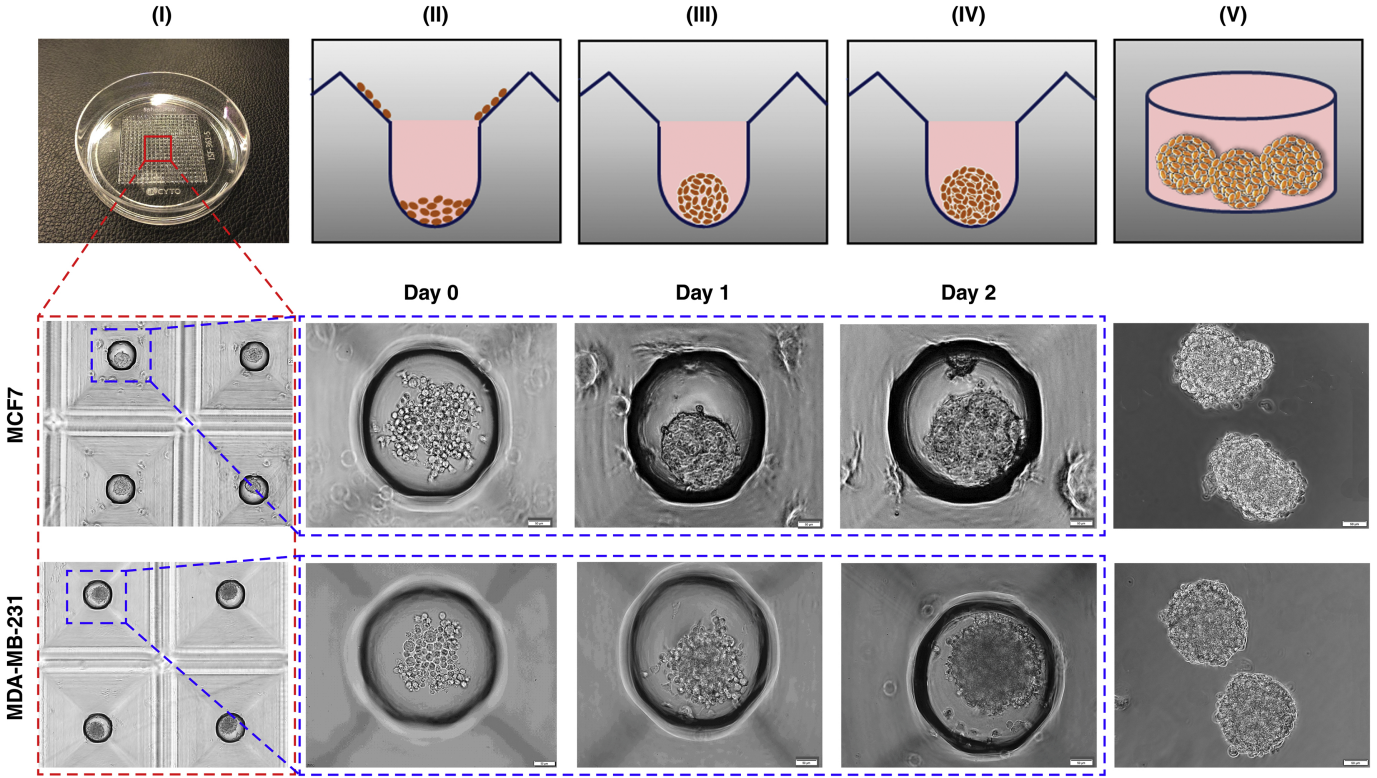

Figure 3

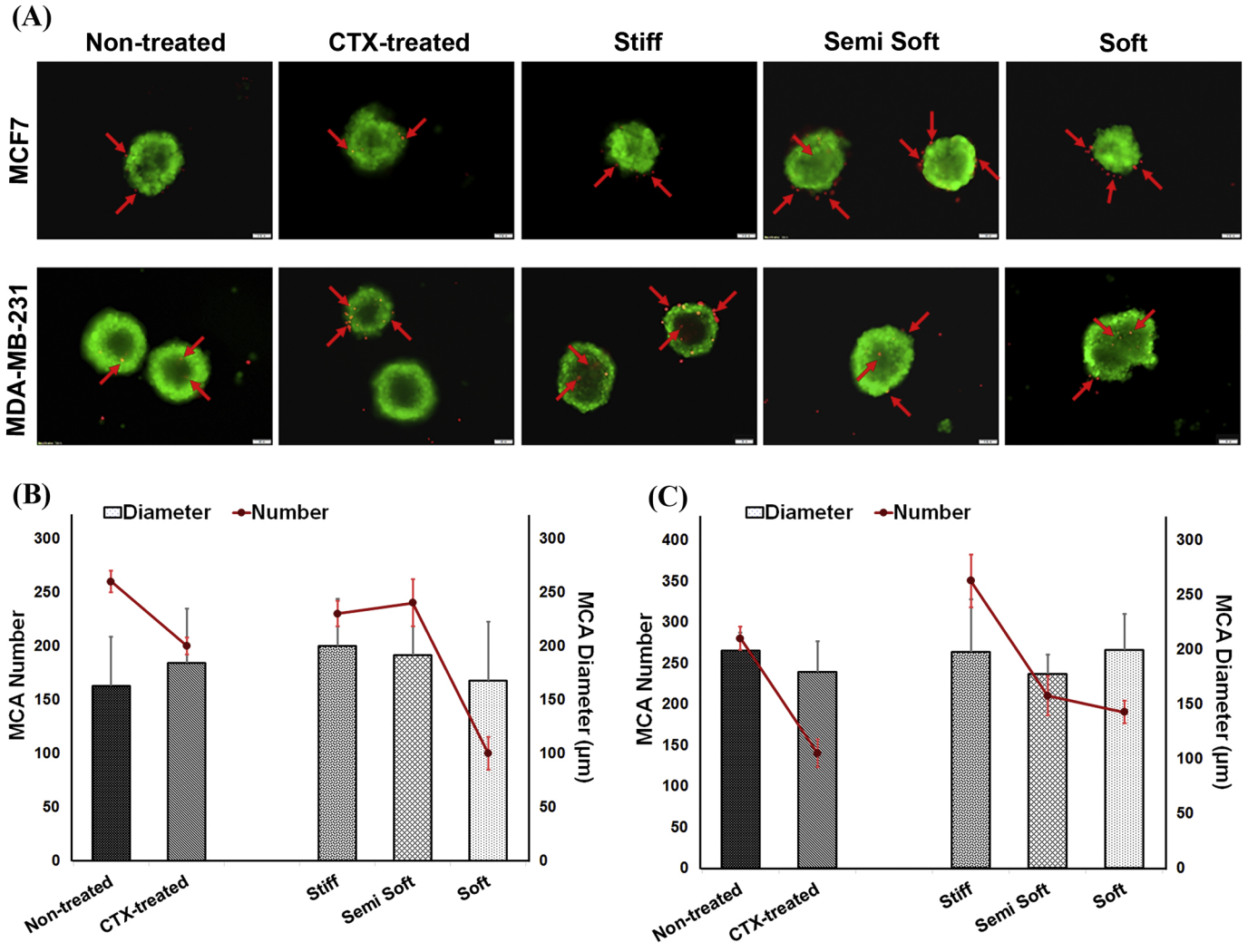
(A)
Non-treated
CTX-treated
Stiff
Semi Soft
Soft
MCF7
MDA-MB-231
(B)
Diameter
Number
MCA Number
MCA Diameter (μm)
Non-treated
CTX-treated
Stiff
Semi Soft
Soft
(C)
Diameter
Number
MCA Number
MCA Diameter (μm)
Non-treated
CTX-treated
Stiff
Semi Soft
Soft

Figure 4

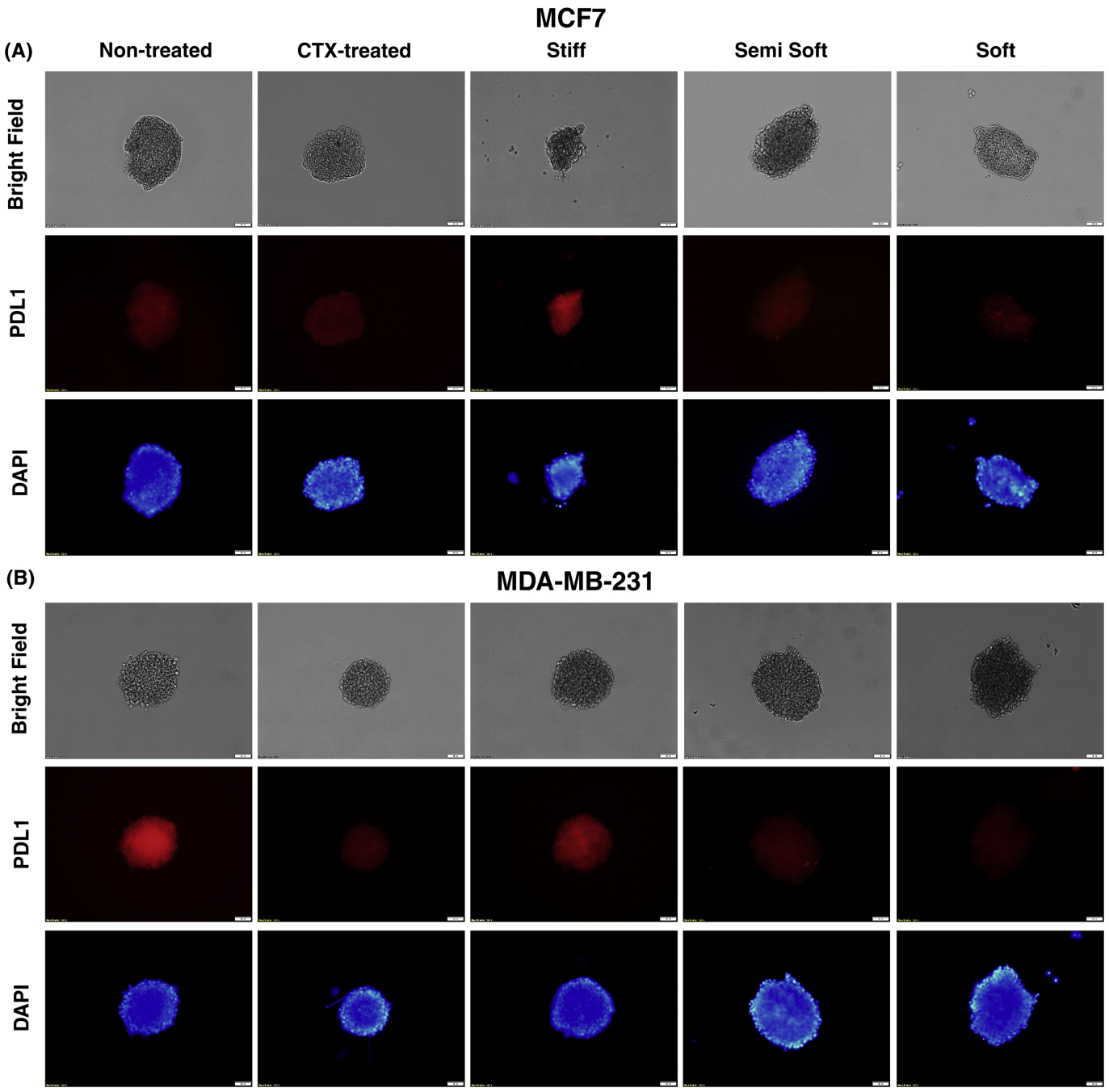
MCF7
(A)
Non-treated
CTX-treated
Stiff
Semi Soft
Soft
Bright Field
PDL1
DAPI
(B)
MDA-MB-231
Bright Field
PDL1
DAPI

Figure 5

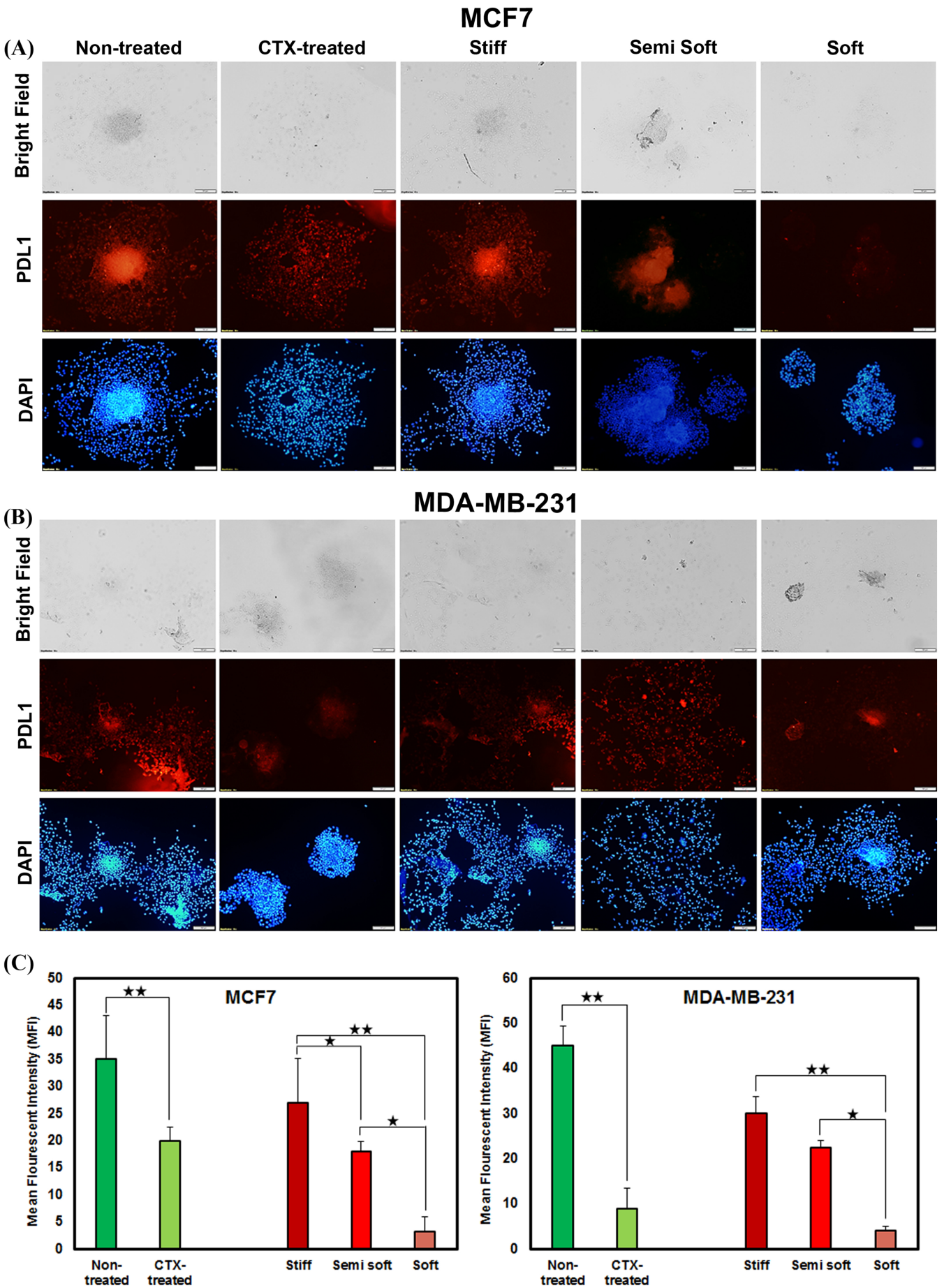
MCF7
(A)
Non-treated
CTX-treated
Stiff
Semi Soft
Soft
Bright Field
PDL1
DAPI
MDA-MB-231
(B)
Bright Field
PDL1
DAPI
(C)
MCF7
Mean Flourescent Intensity (MFI)
Non-treated
CTX-treated
Stiff
Semi soft
Soft
MDA-MB-231
Mean Flourescent Intensity (MFI)
Non-treated
CTX-treated
Stiff
Semi soft
Soft

Figure 6

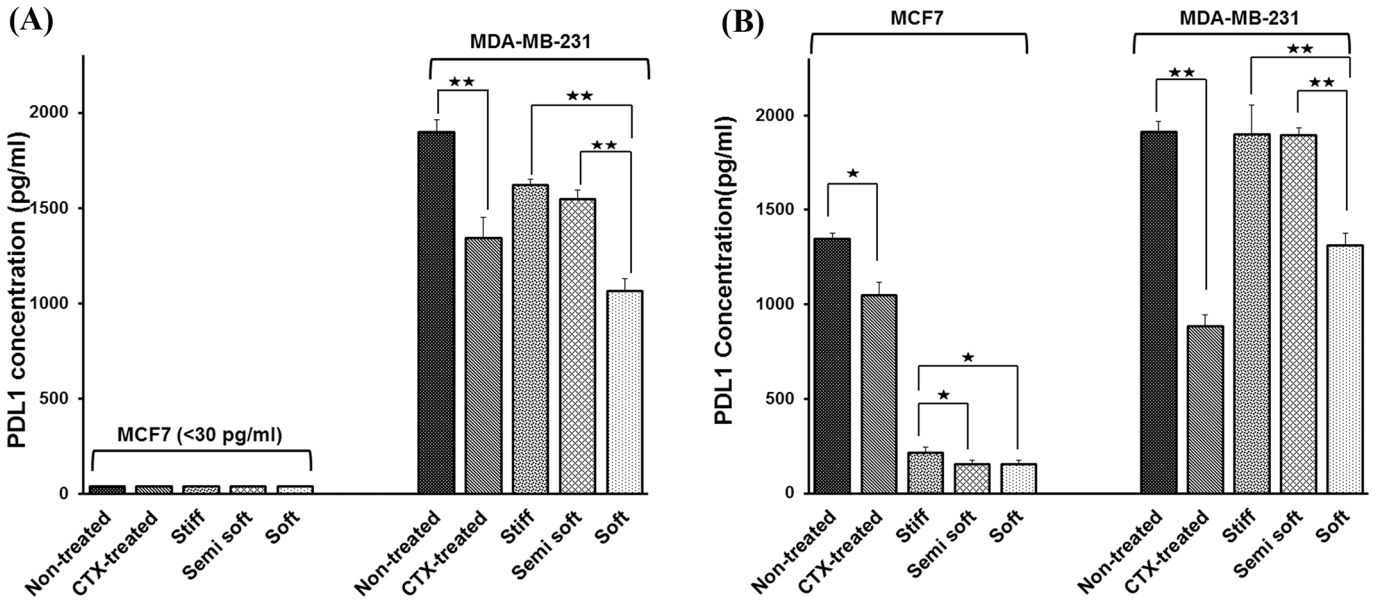
(A)
MDA-MB-231
MCF7 (<30 pg/ml)
PDL1 concentration (pg/ml)
2000
1500
1000
500
0
Non-treated
CTX-treated
Stiff
Semi soft
Soft
(B)
MCF7
MDA-MB-231
PDL1 Concentration(pg/ml)

Figure 7

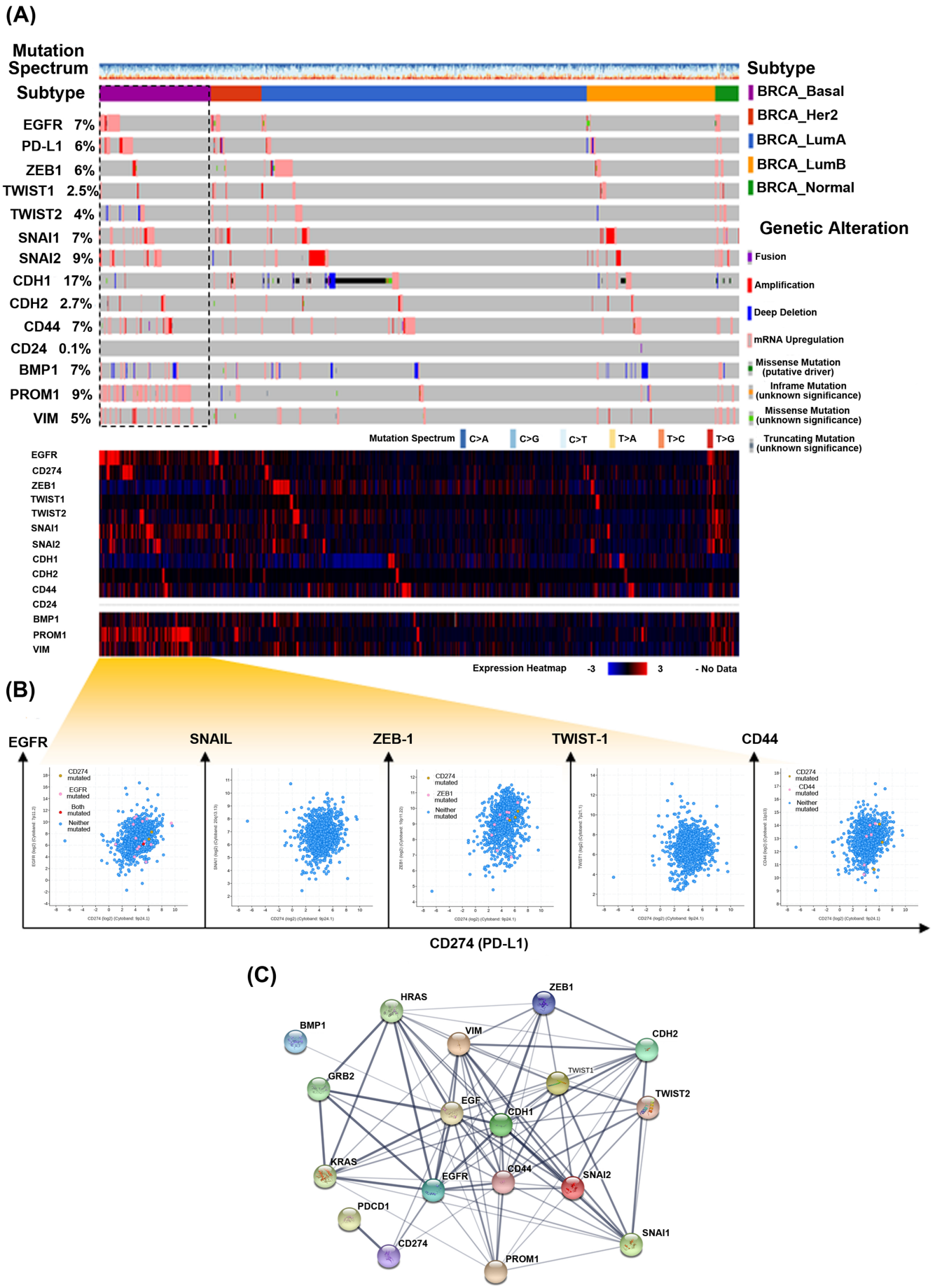
(A)
Mutation Spectrum
Subtype
EGFR 7%
PD-L1 6%
ZEB1 6%
TWIST1 2.5%
TWIST2 4%
SNAI1 7%
SNAI2 9%
CDH1 17%
CDH2 2.7%
CD44 7%
CD24 0.1%
BMP1 7%
PROM1 9%
VIM 5%
Subtype
BRCA_Basal
BRCA_Her2
BRCA_LumA
BRCA_LumB
BRCA_Normal
Genetic Alteration
Fusion
Amplification
Deep Deletion
mRNA Upregulation
Missense Mutation (putative driver)
Inframe Mutation (unknown significance)
Missense Mutation (unknown significance)
Truncating Mutation (unknown significance)
Mutation Spectrum C>A C>G C>T T>A T>C T>G
EGFR
CD274
ZEB1
TWIST1
TWIST2
SNAI1
SNAI2
CDH1
CDH2
CD44
CD24
BMP1
PROM1
VIM
Expression Heatmap -3 3 - No Data
(B)
EGFR
SNAIL
ZEB-1
TWIST-1
CD44
CD274 (PD-L1)
(C)
HRAS
ZEB1
BMP1
VIM
CDH2
GRB2
TWIST1
TWIST2
EGF
CDH1
KRAS
CD44
EGFR
SNAI2
PDCD1
SNAI1
CD274
PROM1

Figure 8